Integration of PV and Battery Storage for Catenary Voltage Regulation and Stray Current Mitigation in MVDC Railways

Salman Aatif, Xiaowei Yang, Hai Hu, Santa Kumar Maharjan, and Zhengyou He

***Abstract*—Innovative advancement in power electronics is reshaping the conventional high-voltage transmission systems and has also opened a new paradigm for researchers to consider its benefits in the railway electrification system (RES). In this regard, the medium-voltage direct current RES (MVDC-RES) is a key area of interest nowadays. In this paper, a secondary energy source (SES) consisting of renewable energies (REs) and energy storage systems (ESSs) is proposed to solve the issues of catenary voltage regulation, rail potential, and stray current in the MVDC-RES. Some of the major integration topologies of the SES are analyzed for MVDC-RES and the most effective one is proposed and implemented. The voltage at the point of connection (PoC) of the SES is used as a reference for controlling different operation modes of REs and ESSs. Moreover, feedforward control is used at the ESS converter to attain the quick response from the batteries for the desired operation. The proposed scheme improves the catenary voltage, and reduces the rail potential and stray current. Besides, the scheme provides higher energy density and reduces line losses. Simulation results are provided to validate the operation modes and advantages of the proposed scheme.**

***Index Terms*—Medium-voltage direct current (MVDC) railway, railway electrification system (RES), catenary voltage regulation, stray current, photovoltaic (PV), energy storage.**

I. Introduction

THE successful implementation of high-voltage direct current (HVDC) technology in conventional power system has enabled the researchers to explore the benefits of direct current (DC) system in high-speed railways (HSRs). In this regard, some researchers have described the basic architecture, advantages, and voltage control schemes for medium-voltage direct current railway electrification system (MVDC-RES) [1]-[4]. Contrary to the urban DC railway electrification system (DC-RES), the MVDC-RES is considered for long-distance HSR corridors. In the MVDC-RES, the catenary becomes a continuous traction line having no neutral sections. The DC technology brings the advantage of less reactance constraints, which helps increase the distance between voltage source converter (VSC) based traction substations (TSSs). Furthermore, in case of a primary VSC-based TSS failure, the power demands of the system can be shared by other TSSs. The photovoltaic (PV) and battery storage consist of DC system hence, can be easily integrated into MVDC-RES without considering the constraints of frequency and phase angle matching as compared with the alternating current RES (AC-RES) [3], [4]. Train loads often generate harmonics, which can be minimized in the MVDC-RES through smart control of VSC technology at TSSs [5].

Although less reactance and no neutral sections in the MVDC-RES offer the advantage of the increased distance between adjacent TSSs, the traction line resistance between the train loads and TSSs is increased, which causes voltage degradation; specifically, at mid-section between two adjacent TSSs [3], [4]. Moreover, the increased traction line resistance also increases the rail potential and in turn increases the stray current. A part of this stray current also flows through the metallic structures embedded in the earth within the vicinity of traction line and causes the corrosion [6].

Meanwhile, the higher penetration of renewable energies (REs) in conventional power systems has transformed the overall energy market. Decreasing the capital cost of REs has enabled countries to set ambitious targets for increasing the share of REs in their energy mix [7]. Besides bringing down the overall carbon emissions, such resources subsequently provide the benefits of no carbon taxes, feed-in tariffs, tax rebates, and the advantage of attaining the renewable portfolio standards [8]. Owing to numerous advantages, efforts are being made for integrating REs and energy storage systems (ESSs) into the RES. Due to dynamic load conditions of the train loads, it is difficult to operate the traction system only through REs and ESSs, but their integration along with stiff grid-connected TSSs offers more choices of resources along with the benefits of voltage regulation and energy management mechanism [9], [10].

In general, the integration of REs or ESSs in railways is mostly performed to solve the issues of RES. In this regard, researchers have described different integration topologies for urban DC and high-speed AC railways [11], [12]. Consid-

Manuscript received: November 13, 2019; accepted: July 17, 2020. Date of CrossCheck: July 17, 2020. Date of online publication: September 15, 2020.

This article is distributed under the terms of the Creative Commons Attribution 4.0 International License (http://creativecommons.org/licenses/by/4.0/).

S. Aatif (corresponding author), X. Yang, H. Hu, S. K. Maharjan, and Z. He are with the School of Electrical Engineering, Southwest Jiaotong University, Chengdu, China, and S. Aatif is also with the Department of Electrical Engineering (Bannu Campus), University of Engineering & Technology (UET), Peshawar, Pakistan (e-mail: salmanatif@uetpeshawar. edu. pk; yxwswjtu@163. com; swjtu_huhai@163.com; gnewasanta@gmail.com; hezy@swjtu.edu.cn).

DOI: 10.35833/MPCE.2019.000155

ering the prospects of the MVDC-RES in HSRs, it is needed to find an effective integration scheme of REs and ESSs into the MVDC-RES.

This paper proposes an effective secondary energy source (SES) integration topology and its operation control scheme in the MVDC-RES. The proposed scheme improves the catenary voltage and mitigates the rail potential and stray current at most significant places along the traction line. Furthermore, feedforward control (FFC) is proposed at ESS converter, which ensures a more rapid response from the batteries in attaining the desired operation mode. The major contributions of this paper are as follows.

1) The issues of catenary voltage sag, rail potential, and stray current in the MVDC-RES are elaborated.

2) The topologies used for the integration of ESS in conventional (urban) DC-RES and AC-RES are analyzed and an effective placement scheme of SES in the MVDC-RES is proposed.

3) The control methodology for the proposed scheme of SES is implemented.

4) The improvement in the catenary voltage and an effective decrease in the rail potential and stray current is validated through simulations. The improved performance of the MVDC-RES in case of loss of a primary VSC-based TSS is also validated.

II. Catenary Voltage, Rail Potential, and Stray Current in MVDC-RES

Considering the resistance of wires and rails from [4], the resistance of catenary system (contact wire and messenger wire) is considered as 0.104 Ω/km, and that of the rail is 0.01365 Ω/km.

A. MVDC Voltage Level

Researchers have suggested different voltage levels for MVDC-RES. References [1], [3], [4] have suggested 24 kV in their simulations, while [2] has suggested 11 kV as the maximum voltage. Most of the conventional HSRs use 25 kV AC voltage as the rated voltage [1]. In order to get the real benefits of the MVDC technology in HSRs, the selected DC voltage must be around 25 kV. It ensures approximately the same currents in the catenary system as in the 25 kV AC-RES, along with the benefits of MVDC technology. Moreover, IEEE 1709-2010 standard describes the 24 kV MVDC voltage level as a future design class for the MVDC systems, which provides the basis for the attainment of protection and other related technologies for 24 kV DC systems in the future [13].

In order to consider a voltage level close to the current AC-RES standard, and to follow the future designated MVDC voltage standard, a 24 kV MVDC-RES is considered for the simulations throughout this paper.

B. Catenary Voltage Degradation in MVDC-RES

The increased distance between the adjacent TSSs in the MVDC-RES results in increased traction line resistance, which causes voltage degradation or sag, specifically, at mid-section between the adjacent TSSs [3], [4]. The issue is validated through the simulations by considering the complete journey of a single moving train on a considered 310 km traction line shown in Fig. 1, where HVAC stands for high-voltage alternating current. Four VSC-based TSSs, 92 km apart from each other, feed the MVDC-RES system. The first and last TSSs also feed the end sections of 17 km. The load voltage profile for a single moving train along the considered traction line is given in Fig. 2. All the simulations are performed in MATLAB/Simulink. The moving train scenario is obtained by varying the traction line resistance at both sides of the train load. The train load is assumed as a constant power load with uniform tractive effort/speed, and reaches its destination without stopping at any station [1], [2], [14], [15]. It can be observed that, as the train reaches the mid-section, the voltage drops below 23 kV. This is mainly because the traction line resistance between the TSSs and train load becomes the maximum.

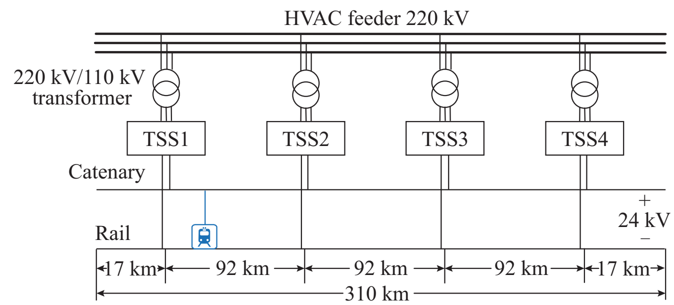

Fig. 1. Layout of considered MVDC traction line.

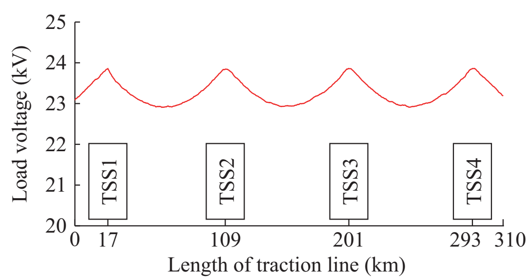

Fig. 2. Load voltage profile of a single moving train along considered traction line.

In [4], the mid-section catenary voltage is adjusted through adaptive droop method at primary VSC-based TSS, which requires a fast and reliable communication link to send the voltage information to the VSC-based TSSs. Different studies about catenary voltage regulation in conventional DC- and AC-RESs are highlighted in Section III.

C. Rail Potential and Stray Current in MVDC-RES

The rail is used as a return path for the load current in DC railways. The return current passing through the rail creates a potential difference between the rail and ground and is generally known as rail potential. The rail potential causes a portion of rail current to leak into the earth, which is known as stray current. A part of this stray current also flows through the metallic structures embedded in the earth, within the vicinity of traction line, and causes the corrosion [6]. For an ideal grounded traction model of DC-RES given in Fig. 3, the total stray current leaking into the earth at any location can be calculated using (1) [16], [17]. In Fig. 3, I_{si} (i = 1, 2, …, n) is the stray current at the i^{th} location; V_{ri} is the voltage developed in the rail at the i^{th} location due to the return current I_r; R_{ri} is the resistance of rails per km; R_{gi} is the rail to ground resistance per km; and R_L is the train load.

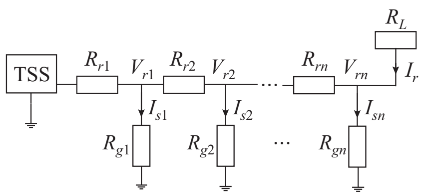

Fig. 3. An ideal grounded traction model of DC-RES.

$$I_{si} = \frac{V_{ri}}{R_{gi}} \tag{1}$$

The stray current and rail to ground voltage at any location along the traction line can be obtained by putting an ammeter in series with R_{gi} and a voltmeter across R_{gi}, respectively. Considering safety requirements from the electric shock, the rail potential must be less than the maximum permissible values given in EN-50122-1. Moreover, to avoid the corrosion due to the stray current in the embedded metallic structures, within the vicinity of traction line, as given in EN-50122-2, the average value of the stray current in DC-RES must not exceed 2.5 mA/m [6]. Figure 4 shows the equivalent circuit of an ideal grounded traction line with two TSSs 92 km apart from each other. The maximum stray current occurs when the train reaches the mid-section (i.e., 46$^{\text{th}}$ km) between the TSSs.

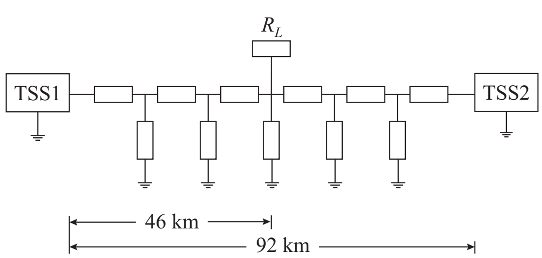

Fig. 4. Equivalent circuit of an ideal grounded traction line in DC-RES.

Considering the rail to ground conductance of 0.01 S/km [18], [19], Figs. 5 and 6 provide the simulation results of rail potential and stray current along the train location for a single moving train, respectively.

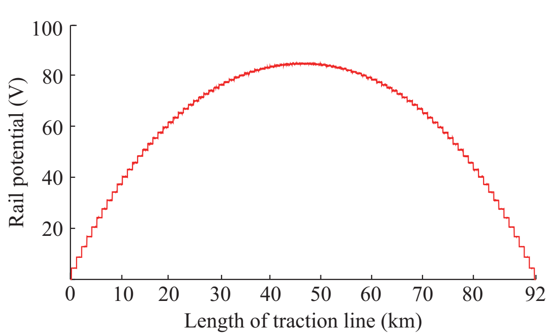

Fig. 5. Rail potential profile of train load for a single moving train.

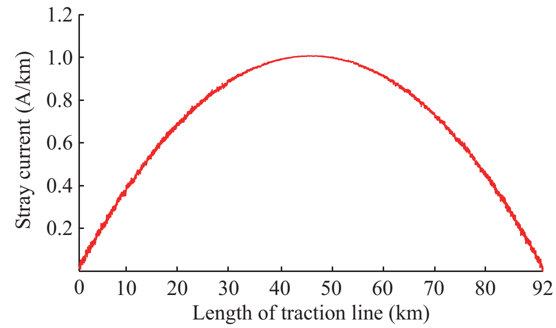

Fig. 6. Stray current profile of train load for a single moving train.

The stray current mentioned in Fig. 6 is the total stray current leaking at the train load. This stray current will be divided into two parts and flow towards TSSs within the earth. The division of the amount of stray current is generally in inverse proportionality to the distance between the considered point and TSS. Simulation results are obtained through the proper switching of resistance modules for catenary resistance, rail resistance, and grounding resistance. Each module has a set of 92 fixed resistances, hence each one represents 1 km section of the traction line.

It is noteworthy that the rail potential and stray current along the train location must always be greater than the average value along the whole rail. The rail potential in Fig. 5 reaches the maximum allowable limit due to the increased traction line distance between the adjacent TSSs. In Fig. 6, the stray current for a single moving train is less than the maximum limit. However, two or more trains on the same rail can increase the current to its maximum allowable limits given in EN-50122-2. Considering the adverse effects of stray current, many techniques have been proposed for its mitigation, which mainly includes decreasing the TSS spacing, increasing the rail to earth resistance, considering the floating scheme, and placing the insulation mats and stray current collection mats [17]-[19]. Most of the proposed techniques are infrastructure-based and are considered for new urban rail transportation projects. The idea of integrating REs and ESSs to mitigate stray current and rail potential would be a new paradigm for futuristic and existing railway systems.

III. ESS Interconnection Scheme for MVDC-RES

The integration of ESSs in electrified railways is generally performed to solve the system issues. Moreover, major aspects regarding the selection of ESSs in the RES are its size (capacity), location, and control scheme [11]. In order to find a potential SES integration scheme to solve the issues of MVDC-RES, a comparative analysis of major existing schemes is made.

In the onboard ESS scheme shown in Fig. 7(a), the ESS, i.e., battery storage or ultra-capacitor, is incorporated into the trains. The control mechanism is usually designed to support the catenary voltage [20]-[22]. This scheme is mostly considered for the DC urban transportation, where the passenger stations are closer, hence there are more regenerative-braking intervals. The MVDC-RES is considered as an alternative to the AC high-speed RES, where the passenger stations are far away from each other and the regenerative-breaking intervals are not frequent. Moreover, the train load is heavier compared with that of the conventional DC-RES. Due to the sizing constraints and less availability of regenerative-breaking intervals, the contributions of the onboard scheme are very limited in terms of catenary voltage support and stray current mitigation in the MVDC-RES.

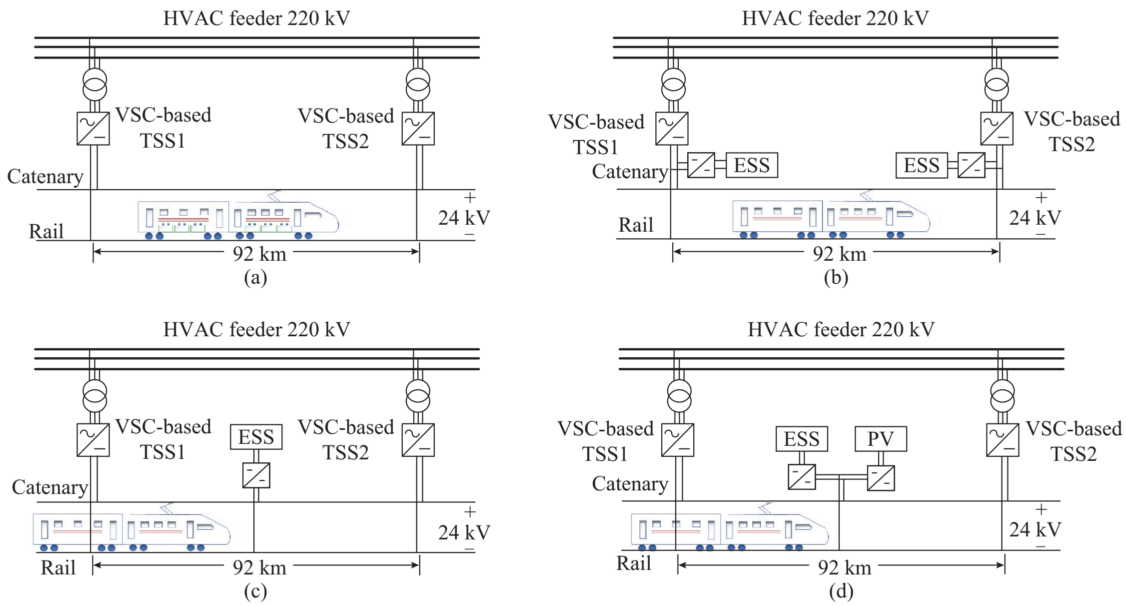

Fig. 7. Major schemes of battery storage in RES. (a) Onboard ESS. (b) ESS at primary VSC-based TSSs. (c) ESS at mid-section between two primary VSC-based TSSs. (d) ESS along with PV at mid-section between two primary VSC-based TSSs.

Figure 7(b) shows the layout of ESS at the primary VSC-based TSSs [23], [24]. A moderate amount of energy can be stored because of no sizing constraints. Also, the integration of REs is possible in this scheme to enhance the energy mix options [25]. The scheme can provide a moderate amount of energy to heavy loads of the MVDC-RES in accelerating mode. Meanwhile, it has no effect on stray current and rail potential mitigation as well as on the catenary voltage regulation at mid-sections. This is mainly because the location and the point of connection (PoC) of the ESS are the same as those of the primary VSC-based TSSs.

Figure 7(c) shows the topology of wayside ESS placed at the mid-section between two primary VSC-based TSSs [11]. Such scheme is mostly used for voltage stabilization along the catenary system in conventional DC-RES or AC-RES [26], [27]. As the power is provided at the mid-section, the length of the traction line between the train loads and TSS decreases, hence the stray current as well as the rail potential decreases. The scheme provides the optimized operation which leads to the minimization of line losses. Moreover, the scheme is free of the sizing constraints of ESS. Despite all the stated advantages, an important challenge related to this scheme is the non-availability of sufficient energy for the ESSs in the MVDC-RES.

The challenge can be resolved by integrating REs such as PVs at these wayside ESSs, as shown in Fig. 7(d). The combination of PVs and ESSs at the mid-section between the primary VSC-based TSSs can serve as an SES in the MVDC-RES. All the discussed schemes are summarized in Table I.

In conclusion, considering the MVDC-RES, on-board ESS scheme has the shortcomings of small capacity, less recharging intervals, and less opportunity for the direct integration of REs with ESS. Similarly, the scheme of ESS at primary VSC-based TSSs has limited voltage regulation ability and has no contribution in the reduction of the rail potential and stray current. In the case of ESS along with PV at the mid-sections, there will be no sizing constraints for ESS and PV units. The PV plant can share its power to the catenary system through converters and can also charge ESS in the case of less demand from train loads. Moreover, the voltage regulation and stray current mitigation can be effectively performed at the most critical locations (mid-sections) along the traction line.

TABLE I
EFFECTIVENESS OF DIFFERENT SCHEMES OF ESS ON CATENARY VOLTAGE REGULATION AND STRAY CURRENT MITIGATION IN MVDC-RES

Scheme	Energy density	Ease of RE integration	Catenary voltage stabilization	Rail potential and stray current mitigation
Onboard ESS	Low	Low	Low	Low
ESS at primary VSC-based TSSs	High	High	Low	None
Wayside ESS at mid-section	Low	High	Low	Low
Wayside ESS along with PV at mid-section	High	High	High	High

Considering the importance of SES in solving the issues of MVDC-RES, there is a great need of implementing an effective control scheme for the operation of SES in the MVDC-RES. Therefore, a control scheme is implemented and simulations are performed in the following sections.

IV. Control Scheme

The layout of MVDC-RES along with SES is given in Fig. 8. The SES consists of PVs and batteries, which is incorporated at mid-section between the primary VSC-based TSSs. Energy exchange is performed by monitoring the voltage at the PoC between the catenary system and SES.

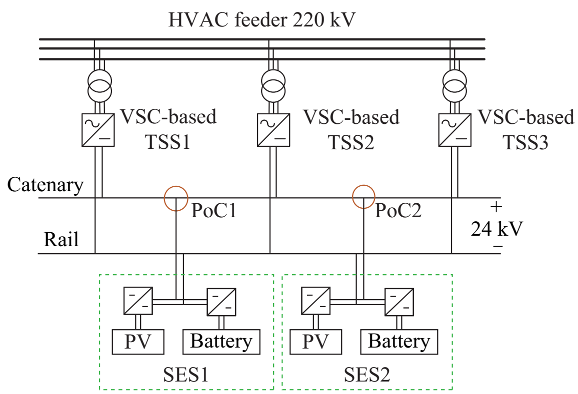

Fig. 8. Layout of SESs at mid-section between primary VSC-based TSSs in MVDC-RES.

Several onboard and wayside ESS schemes discussed in Section III also use the voltage at PoC as a reference to perform the operation of ESS [11], [20], [28]. The control mechanisms for different blocks of the proposed scheme and their operation are discussed as follows.

A. TSS Control

The primary VSC-based TSSs are considered to be the reversible ones, which ensures to feed excess power in the catenary system back to the power grid. Various droop control schemes have been utilized for voltage control of VSC-based TSSs in the MVDC-RES [1], [3], [4]. The main objective of this paper is to propose a placement and control scheme of SES in the MVDC-RES. A conventional droop control scheme with fixed droop value is used for the control of primary VSC-based TSS, as shown in Fig. 9, where PLL stands for phase locked loop, PI stands for proportional-integral, PWM stands for pulse width modulation; $v_{d,ref}$ is the reference voltage given to the VSC-based TSS; i_{TSSi} is the output current; v_{TSSi} is the output voltage; R is the droop value; v_{ref} is the reference voltage for which the TSS is designed (24 kV); E_d, E_q, I_d, I_q are the dq reference frame voltages and currents, respectively; and ωt is the phase angle.

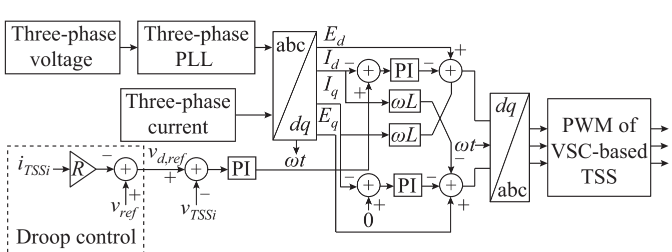

Fig. 9. Control mechanism for primary VSC-based TSS.

Equation (2) represents the conventional droop control scheme [29].

$$v_{d,ref} = v_{ref} - Ri_{TSSi} \tag{2}$$

B. Integration and Control of PV System

In order to get the maximum power from the PV system, the maximum power point tracking (MPPT) control strategy is used to control the output power of the PV system, as shown in Fig. 10. The MPPT control strategy is achieved by utilizing the famous perturb and observe algorithm [30]. For the smooth operation of this strategy, the load must always be greater than the maximum power generated by the PV system; otherwise, the output voltage increases suddenly [31].

In RES, a number of trains always exist on the traction line during day time. Besides, extra power can be shared with the power grid through the primary reversible VSC-based TSSs. Furthermore, constant voltage control is also integrated at the boost converter to ensure the safe operation if the voltage at the PoC increases beyond the maximum allowable limit. In that case, the output voltage becomes constant. However, the maximum output power of the PV system will be compromised. Equation (3) represents the mathematical expression for the constant voltage control scheme given in Fig. 10, where v_p^* is the reference voltage given to the converter for the constant voltage boost operation through the switch control module; $v_{ref,\max}$ is the maximum permitted voltage for the MVDC catenary system; and v_{poc} is the voltage at the PoC between the PV and catenary.

$$v_p^* = k_p(v_{ref,\max} - v_{poc}) + k_i \int (v_{ref,\max} - v_{poc})\mathrm{d}t \tag{3}$$

where k_p and k_i are the proportional and integral coefficients, respectively. It is noteworthy that the traction line always has a number of trains and hence, the PV system will generally follow the MPPT mode. The switch control block monitors v_{poc} and allows the constant voltage mode only if v_{poc} increases beyond $v_{ref,\max}$.

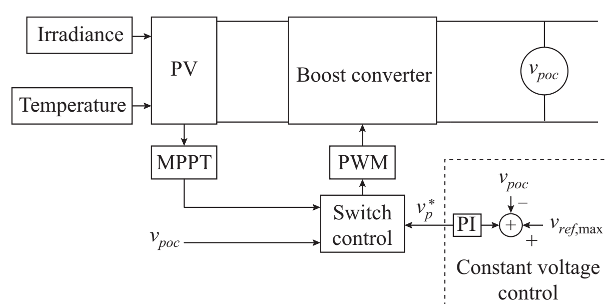

Fig. 10. MPPT control along with constant voltage control for PV system.

C. Integration and Control of ESS

The considered ESS consists of a Li-ion battery set along with bi-directional DC-DC converter. In [23], a simple two-level control is defined either for charging ESS or for supporting catenary voltage. In [31], a variable reference is introduced for different operation modes to achieve an optimized operation in the conventional power system. A similar approach with dynamic reference voltages is applied for the RES in [11]. To effectively solve the issues of MVDC-RES, four-mode control is considered for the battery charging and discharging operation. The selection of each mode depends upon the catenary voltage at PoC and the state of charge (SoC) of the battery set. The operation modes of the battery set against the considered voltage level are given in Table II. The minimum and maximum voltage levels for the safe operation of 24 kV MVDC-RES are 0.76 to 1.1 p.u., i.e., 18.24 to 26.5 kV [1].

TABLE II
OPERATION MODES OF BATTERY SET

Mode	Voltage level (kV)
Charging mode	$v_{poc}>24$
No-operation mode	$23\leq v_{poc}\leq 24$
Voltage enhancement (VE) mode	$20\leq v_{poc}<23$ $(SoC>33\%)$
Contingency mode	$v_{poc}<20$ $(SoC>5\%)$

1) Charging Mode Control

Charging sources for the battery storage system are PVs and braking energy from locomotives. Batteries will be charged when the catenary voltage at PoC increases above 24 kV. To avoid sudden overloading of the catenary system, the charging operation at the battery converter is performed through constant current buck control. For simulations, a simple bi-directional DC-DC converter is used to exchange the power between battery storage system and catenary system. However, for practical analysis, an output-series multilevel dual active bridge (DAB) DC-DC converter must be required in the MVDC-RES. The layout of the control scheme for battery charging mode control of bi-directional DC-DC converter is given in Fig. 11, where i_{kref} is the reference current set for the charging current; i_{bt} is the battery input current; v_{bt} is the battery voltage; and v_{kref} is the reference catenary voltage for the buck operation. The mathematical expression for the operation of constant current buck control is given as:

$$i_k^*=k_p(i_{kref}-i_{bt})+k_i\int(i_{kref}-i_{bt})\mathrm{d}t \tag{4}$$

If the voltage at PoC v_{poc} becomes greater than the reference voltage v_{kref} (24 kV), the switch control block will pass on the PWM switching signal to perform the switching for constant current buck operation. The second control mode is the no-operation or idle one. If the voltage is between 23 kV to 24 kV, the batteries will neither charge nor discharge. A similar no-operation mode is also used in [32]. This makes a barrier and helps to avoid a sudden transition between charging and discharging modes caused by heavy train loads.

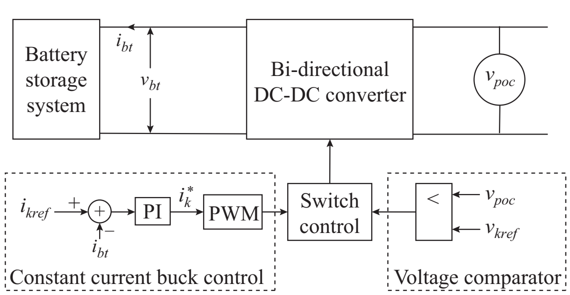

Fig. 11. Charging mode control (buck operation) of bi-directional DC-DC converter.

2) Discharging Mode with FFC

The discharging mode is divided into the VE mode and contingency mode. The layout of the control scheme for battery discharging mode control of bi-directional DC-DC converter for is given in Fig. 12, where v_{biref} (i = 1, 2) is the reference voltage for the boost operation; and i_o is the converter output current. Unlike the charging mode, the discharging mode is determined by two parameters, namely v_{poc} and battery SoC.

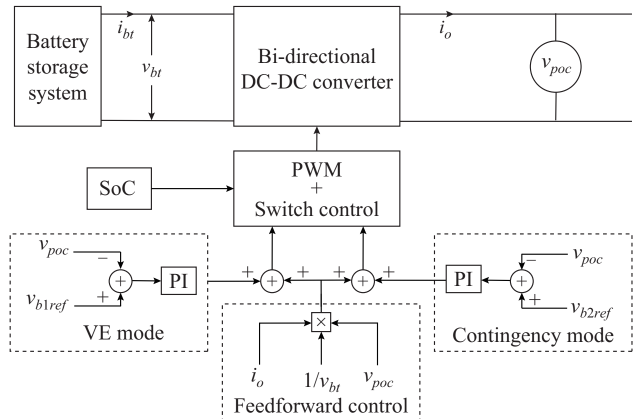

Fig. 12. Battery discharging mode control (boost operation) of bi-directional DC-DC converter.

The VE mode is performed if v_{poc} becomes less than 23 kV and the battery SoC is above 33%. The contingency mode is operated if the voltage goes below 20 kV. Such the control ensures one-third of the battery capacity always remains reserved for contingency situations. The contingency mode of battery storage system greatly improves the performance of RES if a primary TSS is lost (simulated in Section V). The relation for the reference voltage for boost operation is given as:

$$v_{bi}^*=\underbrace{k_p(v_{biref}-v_{poc})+k_i\int(v_{biref}-v_{poc})\mathrm{d}t}_{\text{Voltage control}}+\underbrace{i_o v_{poc}/v_{bt}}_{\text{FFC}} \tag{5}$$

Depending upon the catenary voltage at PoC, the boost converter either operates in VE mode or contingency mode.

The train load is a dynamic load and demands a quick response from the sources feeding it. In order to make a fast response of the boost operation, FFC is incorporated in the control block of boost operation. A similar control scheme has been used in [3] for the primary VSC-based TSSs in the MVDC-RES. The feedforward greatly improves the response time of the battery storage system (simulated in Section V).

V. SIMULATION

In order to validate the effectiveness of the proposed scheme in solving the issues of MVDC-RES, simulations are performed on a 310 km traction line, as shown in Fig. 13. The SESs are incorporated at the mid-section between the primary VSC-based TSSs. The step-down transformers are considered to be included within the TSS block. The parameters of different entities in the system are given in Table III.

All the simulations are performed in MATLAB/ Simulink.

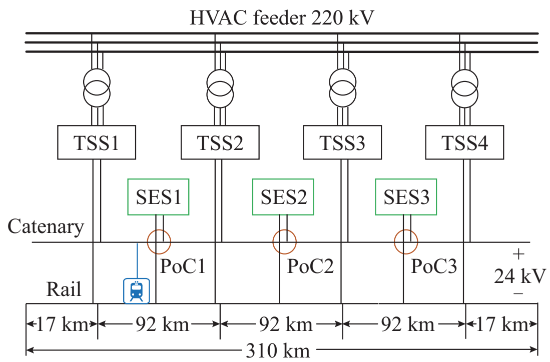

Fig. 13. A 310 km line with four primary TSSs and three SESs.

TABLE III
SYSTEM PARAMETERS IN SIMULATIONS

Parameter	Specification
Transformer at TSSs	220 kV/110 kV
TSS rating	24 kV, 30 MW
VSC topology	3 level
Inductance and capacitance of VSC	10 mH, 4400 μF
Catenary resistance	0.104 Ω/km
Rail resistance	0.01365 Ω/km
Train load	8 MW
Droop value of the TSS	0.3
The maximum capacity of PV plant	8 MW
Total capacity of the Li-ion battery	7.7 MWh
Reference voltage (buck operation)	24 kV
Boost reference voltage for VE and contingency operations	20 kV, 23 kV

Besides the proper placement and control scheme, the other important aspects of designing wayside SESs are the size (capacity) of the PV and battery storage system. The detailed analysis of the SES size requires complete information about the rail traffic timetable as well as the maximum load [24], [33]. As our analysis is related to the placement and control of SES, the maximum capacity of the PV is considered as 8 MW, similar to the load of a single train in the simulations. The maximum size of the Li-ion battery storage system is considered as 7.7 MWh.

A. Voltage Improvement

1) Load Voltage of Single Moving Train

Figure 14 shows the simulation results of load voltage for the complete journey of a single moving train along the traction line. The voltage improvement is observed after the integration of SES into the traction line, which demonstrates the effectiveness of the placement scheme of SES in VSC-based MVDC-RES. The control applied for TSSs, PVs, and battery storage system is the same as that given in Section IV.

2) Catenary Voltage Regulation

For the detailed analysis, 8 trains are randomly distributed along the traction line, as shown in Fig. 15. The PV is an intermittent source of energy and the maximum power cannot be guaranteed all the time. To get a more realistic analysis, the irradiance in this simulation is considered to be 500 wb/m^2, which will make the PVs at all SESs to generate almost half of the full capacity. In order to test all the control scenarios given in Section IV, the battery SoCs of SES1, SES2, and SES3 are considered as 80%, 30%, and 50%, respectively.

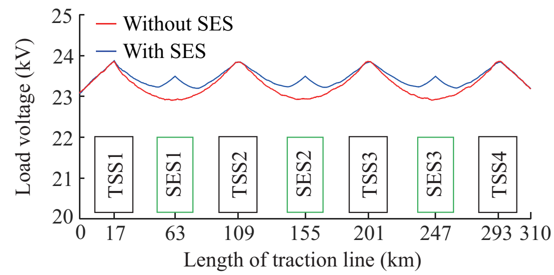

Fig. 14. Load voltages of a single moving train along traction line.

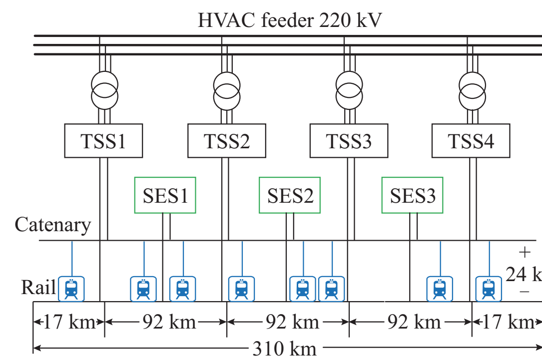

Fig. 15. Eight trains randomly distributed along traction line.

For the train locations mentioned in Fig. 15, the catenary voltage is obtained by observing the voltage at different locations along the traction line, as shown in Fig. 16. The catenary voltage is maintained at 23 kV at the PoC of SES1, which is mainly because the battery set at SES1 has an SoC of 80% and operates in VE mode. The voltage at PoC2 is approximately 22.2 kV. Although the voltage at PoC2 falls in the range of VE mode, the SoC of the battery set at SES2 is 30%. Therefore, no boost operation will perform until the voltage at PoC2 decreases to less than 20 kV.

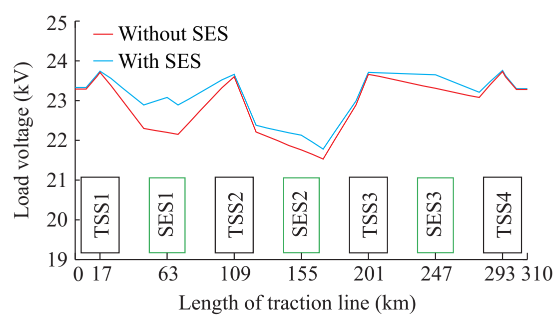

Fig. 16. Catenary voltages for train loads as located in Fig. 15.

The catenary voltage is approximately 23.7 kV at the PoC of SES3. Hence, neither buck nor boost operation is performed as the voltage falls in the range of no-operation mode as discussed in Section IV.

In order to demonstrate the operation of the contingency mode of the battery storage system and observe the effectiveness of FFC, the train locations are changed, as shown in Fig. 17. Considering the batteries have the same SoC as that in the previous case, the batteries at SES2 operate in the contingency mode and keep the voltage at PoC2 above 20 kV, as shown in Fig. 18.

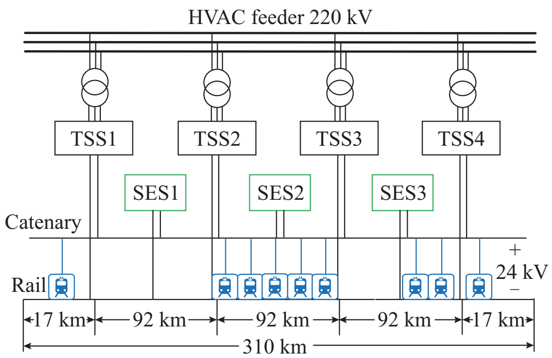

Fig. 17. New train locations along traction line.

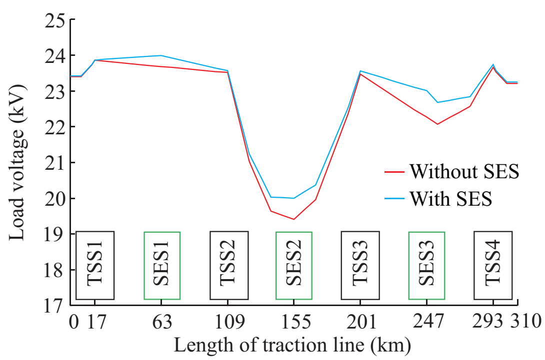

Fig. 18. Catenary voltages after changing train locations as mentioned in Fig. 17.

The catenary voltage at PoC1 is in the range of no-operation mode and hence only PVs feed the power at PoC1. The voltage at PoC3 falls in the range of VE mode and SES3 maintains the voltage at 23 kV.

B. Effectiveness of FFC at ESS Converter

To demonstrate the effectiveness of FFC in enhancing the response of the battery converter, simulations are performed to observe the catenary voltages by changing the train locations from that in Fig. 15 to the one given in Fig. 17. Simulation results for voltage change before the inclusion of the FFC are presented in Fig. 19. Owing to slow response of the PI control, the voltages at PoC2 and PoC3 get adjusted to their respective operation modes after dropping to 19.7 kV and 22.65 kV, respectively.

Figure 20 shows the shift in catenary voltage after the inclusion of FFC at the battery converter. The shift in the voltages at PoC2 and PoC3 is attained quickly at their desired levels without much decrease and delay as compared with the results in Fig. 19.

Hence, the battery storage system with FFC at SESs plays an important role in quickly attaining the desired voltage level for sensitive train loads in the MVDC-RES.

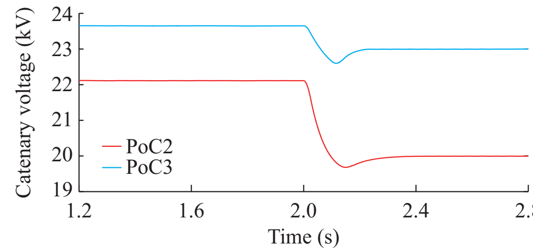

Fig. 19. Shift in catenary voltages at PoC2 and PoC3 after changing train locations (without FFC).

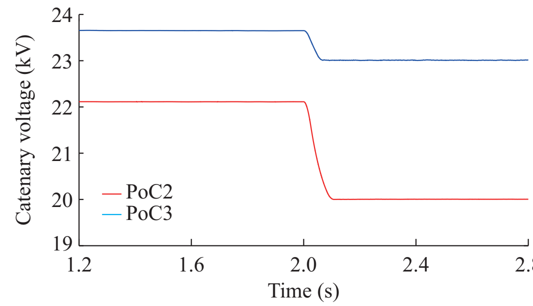

Fig. 20. Shift in catenary voltages at PoC2 and PoC3 after changing train locations (with FFC).

C. Catenary Voltages in the Case of Loss of a Primary VSC-based TSS

The inclusion of SESs at the mid-section between the primary VSC-based TSSs provides considerable support to the catenary voltage in case of loss of a primary VSC-based TSS along the traction line. The worst-case scenario happens when a TSS is lost at the end-section of a traction line [1]. Considering the same train locations as given in Fig. 15 and the same battery SoC as that in Section V-A, Fig. 21 shows the catenary voltages after the loss of TSS4. Without SESs, the voltage at the end-section drops to 17.3 kV approximately. While with the SESs, the voltage at the end-section is maintained at 19.8 kV approximately. In this case, the SES3 works in VE mode as the SoC is greater than 33%.

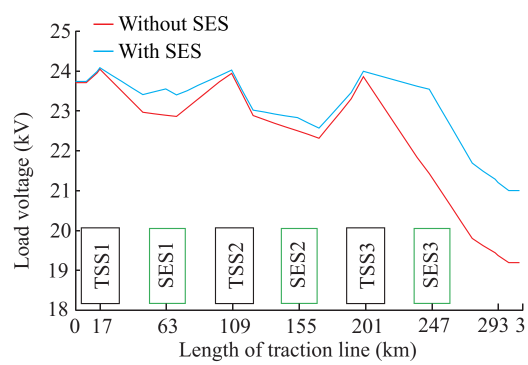

Fig. 21. Catenary voltages with and without SES when a TSS is lost at end-section.

According to Fig. 21, the proper integration of SESs not only enhances the catenary voltage in the normal operation modes but also maintains the minimum operation voltage in the case of loss of a primary VSC-based TSS.

D. Mitigation in Rail Potential and Stray Current

Considering the same traction line specifications as in Section II, simulations are performed for the rail potential and stray current for a single moving train along the traction line between TSS1 and TSS2 in Fig. 4. The simulation results for the rail potential are shown in Fig. 22. The SES is introduced at the mid-section and contributes its share of power to the train loads. The power shared by the SES encounters less traction line resistance as the train moves toward the mid-section. The rail potential is reduced to approximately 20 V at mid-section after the inclusion of SES into the MVDC-RES system. The maximum value of the rail potential becomes 60 V approximately.

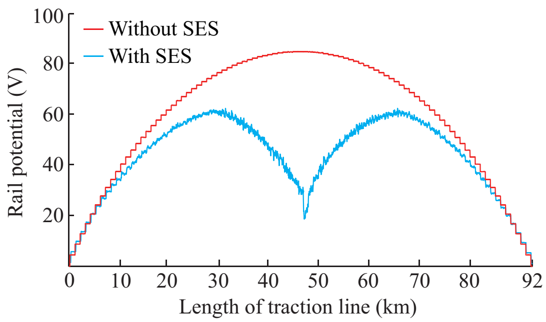

Fig. 22. Rail potential profile at load for a single moving train along traction line between TSS1 and TSS2 in Fig. 4.

The simulation results for the stray current along the train load with and without SES are given in Fig. 23. Considering the same specifications of PVs and battery storage as in previous cases, the maximum value of the stray current for a single moving train is reduced to 0.6 A/km approximately.

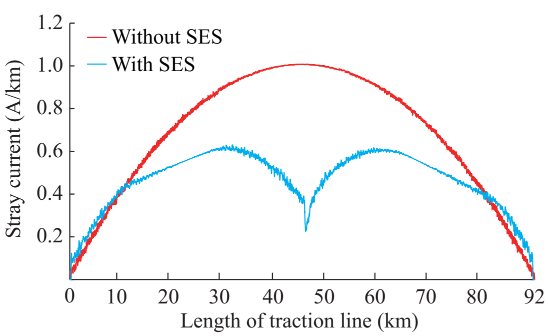

Fig. 23. Stray current profile at load for a single moving train along traction line between TSS1 and TSS2 in Fig. 4.

In summary, the proposed scheme provides a significant reduction in the rail potential and stray current in the MVDC-RES.

VI. Conclusion

The integration of ESSs in electrified railways is generally performed to solve the system issues. In this regard, this paper proposes the topology and control of the SESs for solving the issues of voltage regulation, stray current, and rail potential in the MVDC-RES. The SESs consisting of PV and battery storage system are incorporated at mid-sections between primary VSC-based TSSs. The PV is included to support the essential energy needs of the catenary system and to provide extra power to battery storage system.

Energy exchange is performed by monitoring the voltage at the PoC between the catenary system and SES. The simulations validate the significant improvement in the catenary voltages and a considerable decrease in the stray current and rail potential. Moreover, the proposed scheme also provides a voltage support to the catenary system in the case of loss of a primary VSC-based TSS.

The optimal utilization of the ESS in MVDC-RES is a dynamic problem and requires the information of catenary voltage, rail traffic density (train time table), battery SoC, and weather condition. Considering all the dynamic parameters, the optimal sizing and utilization of the SES (ESS and REs) will be analyzed in the future.

References

[1] A. Gómez-Expósito, J. M. Mauricio, and J. M. Maza-Ortega, "VSC-based MVDC railway electrification system," *IEEE Transactions on Power Delivery*, vol. 29, no. 1, pp. 422-431, Feb. 2014.

[2] A. Verdicchio, P. Ladoux, H. Caron *et al.*, "New medium-voltage DC railway electrification system," *IEEE Transactions on Transportation Electrification*, vol. 4, no. 2, pp. 591-604, Jun. 2018.

[3] X. Yang, H. Hu, Y. Ge *et al.*, "An improved droop control strategy for VSC-based MVDC traction power supply system," *IEEE Transactions on Industry Applications*, vol. 54, no. 5, pp. 5173-5186, Oct. 2018.

[4] S. Aatif, H. Hu, X. Yang *et al.*, "Adaptive droop control for better current-sharing in VSC-based MVDC railway electrification system," *Journal of Modern Power Systems and Clean Energy*, vol. 7, no. 4, pp. 962-974, Jul. 2019.

[5] H. Hu, Z. He, K. Wang *et al.*, "Power-quality impact assessment for high-speed railway associated with high-speed trains using train timetable - Part II: verifications, estimations and applications," *IEEE Transactions on Power Delivery*, vol. 31, no. 4, pp. 1482-1492, Aug. 2016.

[6] A. Ogunsola, A. Mariscotti, and L. Sandrolini, "Estimation of stray current from a DC-electrified railway and impressed potential on a buried pipe," *IEEE Transactions on Power Delivery*, vol. 27, no. 4, pp. 2238-2246, Oct. 2012.

[7] MIT Energy Initiative. (2016, Dec.). Utility of the future. [Online]. Available: http://energy. mit. edu/wp-content/uploads/2016/12/Utility-of-the-Future-Full-Report.pdf

[8] X. Chen, M. B. Mcelroy, Q. Wu *et al.*, "Transition towards higher penetration of renewables: an overview of interlinked technical, environmental and socio-economic challenges," *Journal of Modern Power Systems and Clean Energy*, vol. 7, no. 1, pp. 1-8, Jan. 2019.

[9] S. Boudoudouh and M. Maaroufi, "Renewable energy sources integration and control in railway microgrid," *IEEE Transactions on Industry Applications*, vol. 55, no. 2, pp. 2045-2052, Mar. 2019.

[10] H. C. Kılıçkıran, H. Akdemir, B. Kekezo *et al.*, "Energy management of a smart railway station considering regenerative braking and stochastic behaviour of ESS and PV generation," *IEEE Transactions on Sustainable Energy*, vol. 9, no. 3, pp. 1041-1050, Jul. 2018.

[11] F. Ciccarelli, D. Iannuzzi, K. Kondo *et al.*, "Line-voltage control based on wayside energy storage systems for tramway networks," *IEEE Transactions on Power Electronics*, vol. 31, no. 1, pp. 884-899, Jan. 2016.

[12] S. D'Arco, L. Piegari, and P. Tricoli, "Comparative analysis of topologies to integrate photovoltaic sources in the feeder stations of AC railways," *IEEE Transactions on Transportation Electrification*, vol. 4, no. 4, pp. 951-960, Dec. 2018.

[13] *IEEE Recommended Practice for 1 kV to 35 kV Medium-voltage DC Power Systems on Ships*, IEEE Std 1709-2010, 2010.

[14] X. Zhu, H. Hu, H. Tao *et al.*, "Stability prediction and damping enhancement for MVDC railway electrification system," *IEEE Transactions on Industry Applications*, vol. 55, no. 6, pp. 7683-7698, Dec. 2019.

[15] P. Pan, H. Hu, X. Yang *et al.*, "Impedance measurement of traction network and electric train for stability analysis in high-speed railways," *IEEE Transactions on Power Electronics*, vol. 33, no. 12, pp. 10086-10100, Dec. 2018.

[16] X. Yang, H. Xue, H. Wang *et al*., "Stray current and rail potential simulation system for urban rail transit," in *Proceedings of IEEE International Power Electronics and Application Conference and Exposition*, Shenzhen, China, Nov. 2018, pp. 1-6.
[17] S. A. Memon and P. Fromme, "Stray current corrosion and mitigation: a synopsis of the technical methods used in dc transit systems," *IEEE Electrification Magazine*, vol. 2, no. 3, pp. 22-31, Sept. 2014.
[18] I. Cotton, C. Charalambous, P. Aylott *et al*., "Stray current control in DC mass transit systems," *IEEE Transactions on Vehicular Technology*, vol. 54, no. 2, pp. 722-730, Mar. 2005.
[19] A. Zaboli, B. Vahidi, S. Yousefi *et al*., "Evaluation and control of stray current in DC-electrified railway systems," *IEEE Transactions on Vehicular Technology*, vol. 66, no. 2, pp. 974-980, Feb. 2017.
[20] P. Arboleya, P. Bidaguren, and U. Armendariz, "Energy is on board: energy storage and other alternatives in modern light railways," *IEEE Electrification Magazine*, vol. 4, no. 3, pp. 30-41, Sept. 2016.
[21] S. Hiramatsu, H. Kobayashi, F. P. Wijaya *et al*., "A control method for on board battery power to compensate the fluctuation of line voltage in case of long distance power feeding in DC electric railway," in *Proceedings of 2017 IEEE 12th International Conference on Power Electronics and Drive Systems (PEDS)*, Honolulu, USA, Dec. 2017, pp. 781-788.
[22] M. Steiner, M. Klohr, and S. Pagiela, "Energy storage system with ultracaps on board of railway vehicles." in *Proceedings of 2007 European Conference on Power Electronics and Applications*, Aalborg, Denmark, Sept. 2007, pp. 1-10.
[23] A. Clerici, E. Tironi, and F. Castelli-Dezza, "Multiport converters and ESS on 3-kV DC railway lines: case study for braking energy savings," *IEEE Transactions on Industry Applications*, vol. 54, no. 3, pp. 2740-2750, May-Jun. 2018.
[24] H. Hayashiya, D. Hara, M. Tojo *et al*., "Lithium-ion battery installation in traction power supply system for regenerative energy utilization: initial report of effect evaluation after half a year operation," in *Proceedings of 2014 16th International Power Electronics and Motion Control Conference and Exposition*, Antalya, Turkey, Sept. 2014, pp. 119-124.
[25] J. A. Aguado, A. J. S. Racero, and S. D. L. Torre, "Optimal operation of electric railways with renewable energy and electric storage systems," *IEEE Transactions on Smart Grid*, vol. 9, no. 2, pp. 993-1001, Mar. 2018.
[26] A. Clerici, E. Tironi, and F. C. Dezza, "Voltage stabilization and efficiency improvements on DC railways by stand alone energy storage systems," in *Proceedings of 2017 IEEE International Conference on Environment and Electrical Engineering and 2017 IEEE Industrial and Commercial Power Systems Europe*, Milan, Italy, Jun. 2017, pp. 1-7.
[27] A. Killer, A. Armstorfer, A. E. Díez *et al*., "Ultracapacitor assisted regenerative braking in metropolitan railway systems," in *Proceedings of 2012 IEEE Colombian Intelligent Transportation Systems Symposium (CITSS)*, Bogota, Spain, Aug. 2012, pp. 1-6.
[28] P. Arboleya, B. Mohamed, and I. El-Sayed, "DC railway simulation including controllable power electronic and energy storage devices," *IEEE Transactions on Power Systems*, vol. 33, no. 5, pp. 5319-5329, Sept. 2018.
[29] J. M. Guerrero, J. C. Vásquez, and R. Teodorescu, "Hierarchical control of droop-controlled DC and AC microgrids – a general approach towards standardization," in *Proceedings of 2009 35th Annual Conference of IEEE Industrial Electronics*, Porto, Portugal, Nov. 2009, pp. 4305-4310.
[30] Y. Yusof, S. H. Sayuti, M. A. Latif *et al*., "Modeling and simulation of maximum power point tracker for photovoltaic system," in *Proceedings of National Power and Energy Conference*, Kuala Lumpur, Malaysia, Nov. 2004, pp. 88-93.
[31] K. Sun, L. Zhang, Y. Xing *et al*., "A distributed control strategy based on DC bus signaling for modular photovoltaic generation systems with battery energy storage," *IEEE Transactions on Power Electronics*, vol. 26, no. 10, pp. 3032-3045, Oct. 2011.
[32] R. Barrero, X. Tackoen, and J. V. Mierlo, "Quasi-static simulation method for evaluation of energy consumption in hybrid light rail vehicles," in *Proceedings of 2008 IEEE Vehicle Power and Propulsion Conference*, Harbin, China, Sept. 2008, pp. 1-7.
[33] O. Dutta, M. Saleh, and A. Mohamed, "HESS in DC rail transit system: optimal sizing and system design," in *Proceedings of 2017 IEEE 6th International Conference on Renewable Energy Research and Applications (ICRERA)*, San Diego, USA, Nov. 2017, pp. 908-913.

Salman Aatif received the bachelor's and master's degrees in electrical engineering from University of Engineering & Technology (UET), Peshawar, Pakistan, in 2008 and 2014, respectively. From 2008 to 2015, he worked as a Lecturer at UET. Currently, he is pursuing the Ph.D. degree from Southwest Jiaotong University, Chengdu, China. His research interests include integration of renewable energies and energy storage systems in DC traction power supply system.

Xiaowei Yang received the B.S. degree in electrical engineering from Southwest Jiaotong University, Chengdu, China, in 2016. Currently, he is pursuing the Ph.D. degree in electrical engineering at Southwest Jiaotong University. His research interests include modeling and control, integration of renewable energy source and energy storage systems, and energy management strategy of DC traction power supply system.

Hai Hu received the B.S. degree in electrical engineering from Southwest Jiaotong University, Chengdu, China, in 2019. Currently, he is pursuing the M.S. degree in electrical engineering at Southwest Jiaotong University. His research interests include modeling and control of modular multilevel converter and DC traction.

Santa Kumar Maharjan received the B. Tech. degree in electronic and communication engineering from Uttar Pradesh Technical University, Lucknow, India, in 2007, and the M.Sc. degree in Rail Transit Electrification and Information Technology from Southwest Jiaotong University, Chengdu, China, in 2019. Currently, he is working at the Department of Railways, Nepal. His research interests include stray current control and DC traction power supply system.

Zhengyou He received the B.Sc. and M.Sc. degrees in computational mechanics from Chongqing University, Chongqing, China, in 1992 and 1995, respectively, and the Ph.D. degree in electrical engineering from the School of Electrical Engineering, Southwest Jiaotong University, Chengdu, China, in 2001. Currently, he is a Professor in the School of Electrical Engineering at Southwest Jiaotong University. His research interests include signal process and information theory applied to electrical power system, and application of wavelet transforms in power system.